 Bull. Chem. Soc. Jpn., 76, 1285–1290 (2003)

New Approach to Lowering of the Overvoltage for Oxygen Evolution on RuO_2 and Related Metal-Oxide Electrodes by Ion Implantation

Akira Tsujiko, Kenji Kajiyama,† Masatoshi Kanaya,† Kei Murakoshi, and Yoshihiro Nakato*

Department of Chemistry, Graduate School of Engineering Science, Osaka University, Toyonaka, Osaka 560-8531

†Ion Engineering Research Institute, Hirakata, Osaka 573-0128

(Received November 28, 2002)

The ion implantation method is applied to the improvement of the oxygen-evolution activity for metal oxide electrodes. The implantation of metal ions such as Co^+, Zn^+, and Ru^+ into nanocrystalline RuO_2 and $Ru_xTi_{1-x}O_2$ ($x = 1/2$ and $2/3$) film electrodes caused negative shifts of current density (j) vs potential (U) curves for oxygen evolution by about 20–100 mV, indicating the lowering of the overvoltage for oxygen evolution. Detailed experiments have shown that the lowering of the overvoltage is neither due to a change in the chemical composition of the electrode surface nor due to an increase in the effective area of the electrode surface, but rather is due to production of certain crystal defects (such as atomic gaps) that can act as active sites for oxygen evolution. The result is of much interest, suggesting that the control of surface defect structures is a promising approach for the improvement of the oxygen evolution activity.

Electrolysis of water into hydrogen and oxygen is one of the key reactions in energy conversion technologies. Although hydrogen evolution reaction proceeds efficiently on some precious metal electrodes such as platinum,[1] the oxygen evolution reaction has a fairly high overvoltage of about 0.2 V even for the most active electrodes thus far known, such as RuO_2,[2–4] thus resulting in a serious loss in the energy conversion efficiency. For realizing an efficient energy conversion system based on solar electrolysis,[5] it is of key importance to lower (or to discover an effective method to lower) the overvoltage for oxygen evolution reaction.

A number of studies have been made to find active electrode materials for oxygen evolution reaction. Various metal oxides, such as Co_3O_4,[6] $Mn_xCo_{3-x}O_4$,[7] $Co_xFe_{3-x}O_4$,[8] IrO_2,[9] $Ni_xAl_{1-x}Mn_2O_4$,[10] $LaNiO_3$,[11] Rh_2O_3,[12] PdO,[12] NiO,[12,13] and metal-doped SnO_2,[14] have been investigated usually under the concept of activity improvement by changes of the chemical composition (or the electronic structure) of electrode materials. For RuO_2, the preparation conditions have been studied in detail to get higher activity.[15–17] For oxygen evolution from seawater, (Mn-W)O_x electrodes with high overvoltages for chlorine evolution have been studied.[18] Little attention has, however, been paid to the activity improvement by changes in the morphological (or defect) structure of the electrode surface.

It is well known that crystalline defects at the electrode surface, such as steps and kinks, act as active sites for electrochemical reactions. Theoretically, another-type defects, i.e., defects such as atomic gaps exposed to the surface (see Fig. 1) are expected[19–21] to act as more active sites, especially for oxidation of small-sized species such as H_2O and OH^-. In general, a large change in the electric charge occurs for a reacting species in the oxidation reaction, accompanied by a large change in the electric polarization of the surrounding medium. For the oxidation reaction of a species like OH group at the surface which is in contact with a polar solvent (like water), the reaction causes a large change in the *orientation* polarization of surrounding solvent molecules, similarly to the case of the oxidation reaction in a polar solvent. This results in a large reorganization energy (in Marcus theory) and hence to a large activation energy (or overvoltage). On the other hand, for the oxidation of a species like OH group within the atomic gaps, the reaction only (mainly) causes a change in the *electronic* polarization of the surrounding solid electrode materials that leads to no increase in the reorganization (and activation) energy, because ionic species within the atomic gaps are mainly stabilized by the electronic polarization of the solid electrode materials. Thus, a species within the atomic gaps is more easily oxidized than that at the surface, or in other words, the atomic gaps can act as active sites for electrochemical oxidation–reduction reactions.

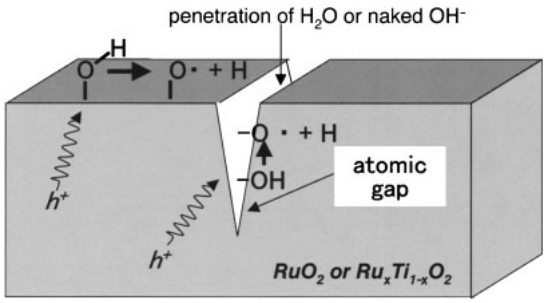

Fig. 1. Schematic illustration of electrochemical oxidation in the bulk-type defects (such as atomic gaps) as compared with that at the surface, with surface OH groups taken as an example of oxidized species.

In the present work, the above idea was investigated by using the ion implantation method, which can introduce

bulk-type defects such as atomic gaps near the electrode surface. Experiments have shown that the control of defect structure near the electrode surface is a promising approach for the improvement of the oxygen evolution activity.

Experimental

Nanocrystalline RuO_2 and $Ru_xTi_{1-x}O_2$ films, into which the ion implantation was carried out, were prepared on Ti-metal plates as a substrate. First, colloidal RuO_2 and $Ru_xTi_{1-x}O_2$ solutions were prepared by controlled hydrolysis. For RuO_2 solutions, 20 mL of 5% HCl containing 8.2 mM $RuCl_3$ (Aldrich reagent grade as $RuCl_3 \cdot 6H_2O$) was slowly added to 10 mL 2-propanol (Aldrich anhydrous grade) at 60 °C with vigorous stirring under N_2 gas flow. The mixture was then kept at 60 °C for 3 h, aged at 4 °C for 24 h, and dried. The resulting RuO_2 white powder was again dispersed in dry ethanol. The transparent colloidal RuO_2 ethanol solutions thus prepared gave more active film electrodes than those prepared with no drying process. For $Ru_xTi_{1-x}O_2$ solutions, 10 mL ethanol dissolving appropriate amounts of $RuCl_3$ and $TiCl_4$ (Aldrich reagent grade) was slowly added to 0.1 M HNO_3. The resultant colloidal $Ru_xTi_{1-x}O_2$ solutions were used for film formation without any drying process.

The colloidal RuO_2 and $Ru_xTi_{1-x}O_2$ solutions were then applied on Ti plates (Nippon Sheet Glass Co. Ltd.) with a spin coater at 2000 rpm. The RuO_2 coated Ti plates were heated at 80 °C for 15 min, and further heated at 300 °C for 15 min. This procedure was repeated several times to get a sufficient film thickness. The RuO_2 films thus prepared were finally heated at 300 °C for 4 h in air. The Ti plates were washed with boiling acetone and pure water before use. The $Ru_xTi_{1-x}O_2$ coated Ti plates were heated at 150 °C for 10 min, and the procedure was repeated several times. The films were finally heated at 600 °C for 2 h in air.

Single crystal TiO_2 (rutile) wafers, as a reference sample, were obtained from Earth Chemical Co., Ltd. They had an area of 10 mm × 10 mm and a thickness of 1.0 mm, and (110)-cut and alkali-polished surfaces. They were used after washing with pure water.

The ion implantation was carried out in Ion Engineering Research Institute, Osaka, Japan, with a 200-keV ion implantation apparatus (B) for an acceleration energy of 5 or 10 keV and with a 200-keV ion implantation apparatus (C) for an acceleration energy of 100 keV. The damage density profiles were calculated using the conventional transportation-in-matter (TRIM) method.[22,23]

Current density (j) vs potential (U) curves were obtained with a commercial potentiostat and a potential programmer, using a Pt plate as the counter electrode and an Ag/AgCl/KCl(sat.) electrode as the reference electrode. The RuO_2 or $Ru_xTi_{1-x}O_2$ film electrodes, as the working electrode, were prepared by attaching a copper wire on an edge of the metal-oxide film with silver paste, followed by covering the whole part, except the 1.0 × 1.0 cm^2 film area, with epoxy resin for insulation. The temperature of the electrolyte solution was kept at 25 °C. Nitrogen gas was bubbled through the electrolyte under stirring. Electrolyte solutions were prepared using highly pure Milli-Q water and reagent grade chemicals without further purification.

Surface inspection of RuO_2 or $Ru_xTi_{1-x}O_2$ films was carried out with a Hitachi S-5000M scanning electron microscope (SEM) and a Hitachi HF-2000 transmission electron microscope (TEM). TEM samples were prepared by the FIB (focused ion beam) method,[24] using a Ga^+ ion beam. For TEM inspection, selected area electron diffraction (SAED) measurements were done at the same time, with the beam diameter of 2–3 nm. The X-ray photoelectron spectra (XPS) were obtained with a Shimadzu ESCA-1000 spectrometer, using an Mg Kα line.

Results

The RuO_2 and $Ru_xTi_{1-x}O_2$ films used in the present work were composed of nanocrystalline particles of about 10–20 nm in diameter, and had the thickness of about 1.5 μm. Figure 2 shows, as an example, (A) an SEM image of the surface and (B) a TEM image of the cross section for a RuO_2 film.

Figure 3 compares log j vs U (Tafel) plots in the potential region of oxygen evolution for several RuO_2 film electrodes in 1.0 M NaOH at 25 °C. The j–U curve for Ru^+-ion implanted RuO_2 (open circle) is shifted in potential by about 20–40 mV toward the negative compared with that for as-prepared (non-implanted) RuO_2 (triangle). The Ru^+-ion implantation was carried out at an acceleration voltage of 10 kV with a dose of 1.0×10^{15} cm^{-2}. It is to be noted that the curve for the non-implanted RuO_2 (triangle) in the present work agrees with the most efficient curve reported for nanocrystalline RuO_2 film electrodes (rectangle),[4] implying that the ion implantation truly improves the oxygen evolution activity for RuO_2. A j–U curve for a Pt electrode (rhombus) is included in Fig. 3 for reference.

Figure 4(A) shows the dependence of the j–U curve for the Ru^+-ion implanted RuO_2 film electrodes on the acceleration voltage in a range of 5 to 100 kV, under a constant dose of 1.0×10^{15} cm^{-2}. The most efficient characteristic is obtained at around 10 kV. Figure 4(B) shows the dependence of the j–U curve on the dose of the ion beam in a range of 0.2×10^{15} to

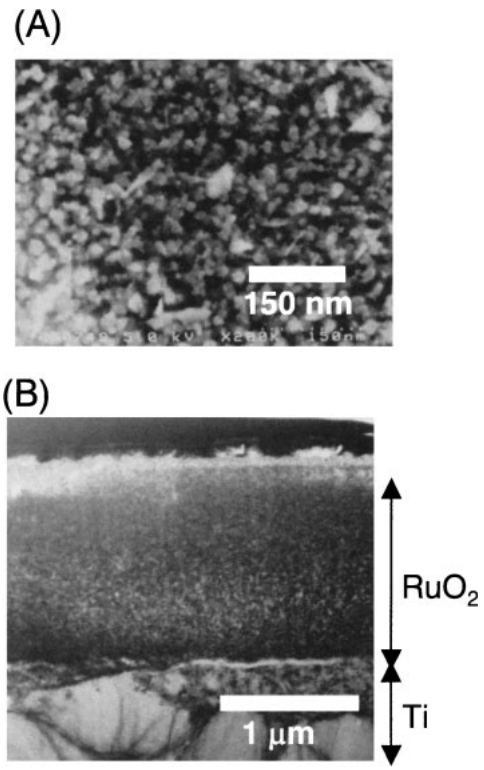

Fig. 2. (A) An SEM image of the surface and (B) a TEM image of the cross section for a nanocrystalline RuO_2 film.

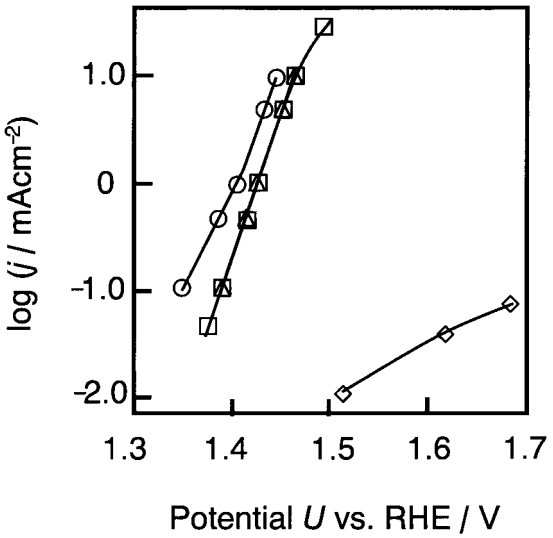

Fig. 3. Log j vs U plots for nanocrystalline RuO_2 film electrodes in 1.0 M NaOH at 25 °C. Open circle (○) is for Ru^+-ion implanted RuO_2 (10 kV, 1.0×10^{15} cm^{-2}), and triangle (△) is for as-prepared (non-implanted) RuO_2. Rectangle (□) and rhomb (◇) indicate reported data[4] for as-prepared nanocrystalline RuO_2 and polycrystalline Pt, respectively.

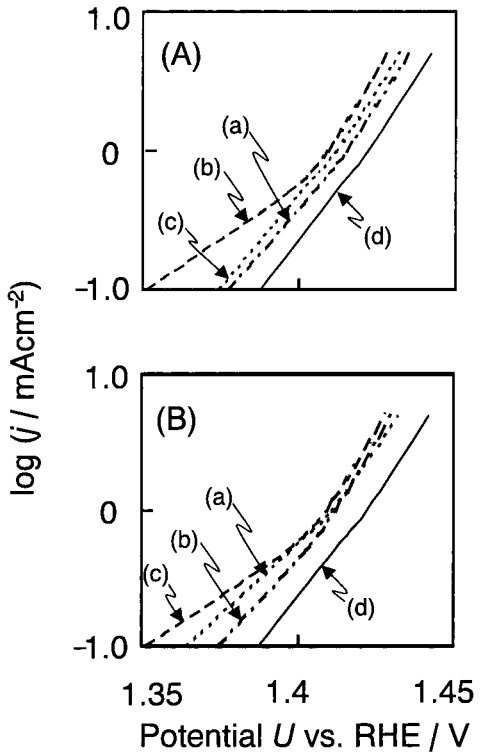

Fig. 4. Dependences of the j–U curve for Ru^+-ion implanted RuO_2 film electrodes on the acceleration voltage (V_{ac}) and the dose (D) of the ion beam. In (A), V_{ac} is (a) 5 kV, (b) 10 kV, and (c) 100 kV, with a constant dose of 1.0×10^{15} cm^{-2}. In (B), D is (a) 0.2×10^{15} cm^{-2}, (b) 0.5×10^{15} cm^{-2}, and (c) 1.0×10^{15} cm^{-2}, with a constant V_{ac} of 10 kV. Curve (d) is for non-implanted RuO_2, both in (A) and (B). The electrolyte is 1.0 M NaOH at 25 °C.

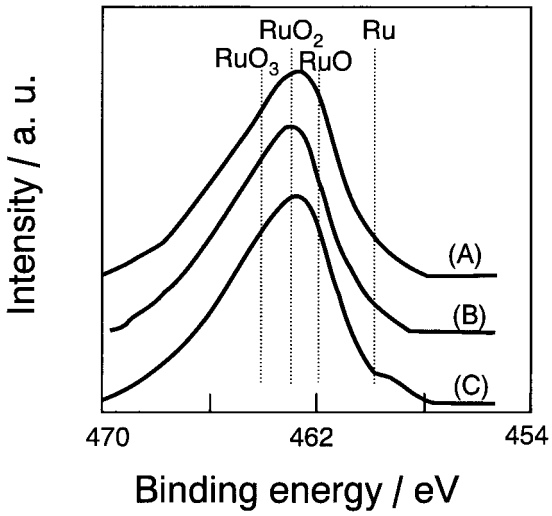

Fig. 5. XPS spectra in the Ru 3p region for (A) non-implanted and (B) Ru^+-ion implanted (10 kV, 1.0×10^{15} cm^{-2}) RuO_2 film electrodes after oxygen evolution experiments were done. Spectrum (C) is for the Ru^+-ion implanted RuO_2 film before the oxygen evolution experiment.

1.0×10^{15} cm^{-2}, under a constant acceleration voltage of 10 kV. The shift in the j–U curve appears to become larger as the dose increases, though the order is reversed for the doses of 0.2×10^{15} and 0.5×10^{15} probably because the shift will also be influenced by geometrically rough surface structures of particulate RuO_2 films, which are different from sample to sample.

Figure 5 shows XPS spectra in the Ru 3p region for (A) a non-implanted and (B) a Ru^+-ion implanted (10 kV, 1.0×10^{15} cm^{-2}) RuO_2 film electrode, both after electrochemical oxygen-evolution experiments (such as in Fig. 3) were done. Spectrum (C) is for the Ru^+-ion implanted RuO_2 film before the oxygen evolution experiment. Spectra (A) and (B) have a peak at the peak position for RuO_2, with no peak or shoulder at the peak positions for Ru, RuO, and RuO_3, suggesting that both the non-implanted and Ru^+-ion implanted RuO_2 films after the oxygen evolution experiments are really composed of RuO_2. On the other hand, spectrum (C) shows a weak peak at the peak position for Ru metal, indicating that the film just after the Ru^+-ion implantation contains a small amount of Ru metal.

The above result suggests that the negative shifts in the j–U curves by the Ru^+-ion implantation are not caused by a change in the chemical composition of the films but by production of certain damage (crystal defects) in the films. This expectation is supported by the fact that the calculated damage density profiles can explain the acceleration-voltage dependence of the j–U curves in Fig. 4(A). The calculation was carried out for RuO_2 single crystals (with no consideration of occurrence of sputtering) by using the TRIM method,[22,23] in which a collision of a Ru^+ ion with a Ru or O atom in RuO_2 crystal is assumed to produce one defect. As shown in Fig. 6, the maximum of the calculated damage density profiles for 5 and 10 kV lies close (about 8 and 10 nm respectively) to the surface, whereas that for 100 kV is rather far (about 35 nm) from the

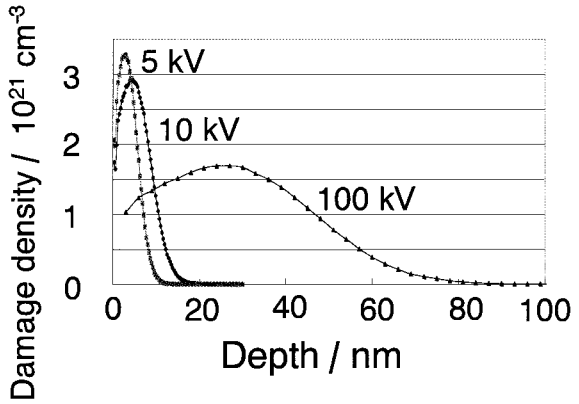

Fig. 6. Damage density profiles for Ru^+-ion implanted RuO_2 crystals, calculated by the TRIM method. The calculation was done for acceleration voltages of 5, 10, and 100 kV, with a constant dose of 1.0×10^{15} cm^{-2}.

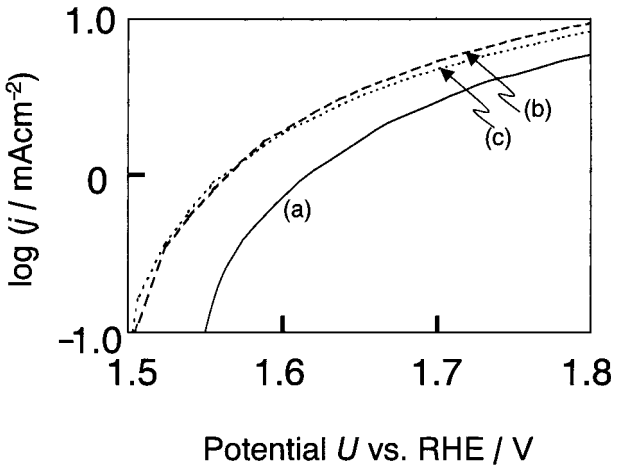

Fig. 7. Log j vs U curves for (a) non-implanted, (b) Zn^+-ion implanted, and (c) Co^+-ion implanted $Ru_{2/3}Ti_{1/3}O_2$ nanocrystalline film electrodes in 1.0 M NaOH at 25 °C. The ion implantation was carried out at 10 kV and 5.0×10^{15} cm^{-2} for both Co^+ and Zn^+ ions.

surface. The ineffectiveness of the 100-kV implantation in Fig. 4(A) can thus be explained as being due to the fact that only defects produced close to the surface are effective for the improvement in the electrochemical activity. The ineffectiveness of the 5-kV implantation can be attributed to the fact that ions of too low energy such as 5 keV are apt to cause surface sputtering rather than ion implantation.[25]

We did similar experiments for $Ru_xTi_{1-x}O_2$ film electrodes, where x is 1/2 or 2/3. Fairly large negative shifts in the j–U curves by ion implantation, exceeding 100 mV, were observed for such mixed-oxide electrodes under appropriate conditions, though the mixed oxide electrodes themselves are less active for oxygen evolution than the RuO_2 electrodes.

Figure 7 shows the dependence of the j–U curves for the $Ru_{2/3}Ti_{1/3}O_2$ electrode on the kind of implanted ions. The j–U curves for the Co^+- and Zn^+-ion implanted electrodes nearly agree with each other, both being shifted toward the negative from that for the non-implanted electrode. As the electrochemical properties of Co and Zn are quite different, this result again indicates that the negative shifts in the j–U curves are not due to a change in the chemical composition of the films but due to production of damages. In fact, the calculation has shown that Co^+ and Zn^+ ions with the same mass number produce nearly the same damage density profiles, as shown in Fig. 8.

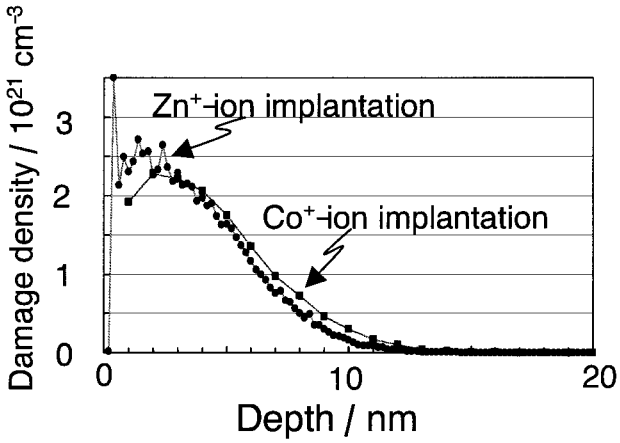

Fig. 8. Damage density profiles for Co^+- and Zn^+-ion implanted TiO_2 crystals, calculated by the TRIM method. The calculation was done for an acceleration voltage of 10 kV and a dose of 1.0×10^{15} cm^{-2}.

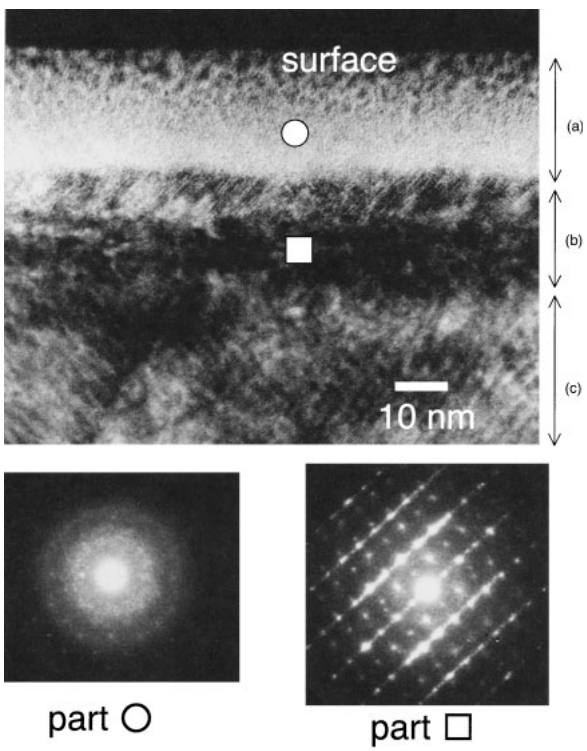

Fig. 9. Cross-sectional TEM image (upper figure) for a Ru^+-ion implanted RuO_2 nanocrystalline film, together with SAED patterns (lower figures) for two areas designated by open circle and rectangle in the TEM image. The ion implantation was carried out at 10 kV and 1.0×10^{15} cm^{-2}.

Figure 9 shows a cross-sectional TEM image for a Ru^+-ion implanted RuO_2 film, together with SAED (selected area elec-

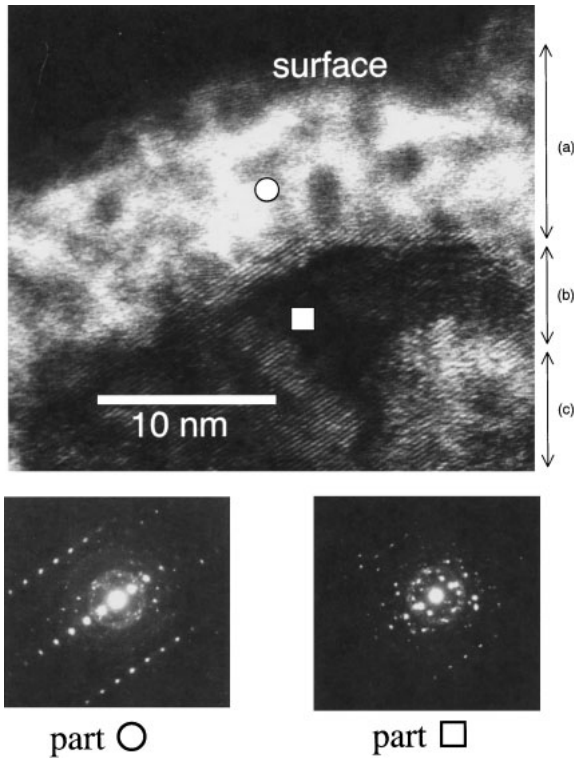

Fig. 10. Cross-sectional TEM image (upper figure) for a Ti^+-ion implanted TiO_2 single crystal, together with SAED patterns (lower figures) for two areas designated by open circle and rectangle in the TEM image. The ion implantation was carried out at 10 kV and 2.0×10^{15} cm^{-2}.

tron diffraction) patterns for two areas marked by a circle and a rectangle in the TEM image. It is known[25] that the ion implantation in general produces two surface layers, the uppermost damaged layer and the second uppermost ion-implanted layer. The TEM image in Fig. 9 indeed indicates the formation of two surface layers, designated by (a) and (b), each having the thickness of about 10 nm. The TEM image for the uppermost surface layer (a) shows almost no lattice image, contrary to the underlying parts (b) and (c). However, the SAED pattern for the layer (a) shows fringed concentric rings together with ordered spots, suggesting that the layer (a) is composed of multi-cracked crystalline or disordered microcrystalline domains.

Figure 10 shows, for reference, results of similar experiments to above for single crystal TiO_2, for which, contrary to the case of nanocrystalline films (Fig. 9), the effect of the ion implantation on the surface structure will be more easily understood. TiO_2 single crystal is chosen because its crystal properties are similar to those for RuO_2 and no RuO_2 single crystal is available. Figure 10 shows essentially the same results as Fig. 9, indicating that the above-mentioned interpretation for Fig. 9 is reasonable.

Discussion

Though it is likely that the morphologically rough surface structures of the nanocrystalline RuO_2 film electrodes more or less influence the experimental results such as the shifts in the j–U curves, it is evident from Figs. 3, 4, and 7 that the ion implantation causes the negative shifts in the j–U curves indicative of the improvement of the oxygen-evolution activity of the electrodes. The experimental results also show that the activity improvement is not caused by a change in the chemical composition of the electrodes but by production of certain damage (crystal defects) acting as active sites, as mentioned in the preceding section. It is to be noted also that the Ru^+-ion implanted RuO_2 electrode has the higher activity than the RuO_2 electrode itself that has thus far been known to be the most active (Figs. 3 and 4).

What kinds of damage (or crystal defects) do act as active sites for oxygen evolution? First it is to be noted that we can exclude a possibility that the negative shift in the j–U curve is caused by an increase in the effective area of the electrode surface by ion implantation. If the negative shift were caused by such an increase in the effective surface area, the current density $j_{imp}(U)$ for an ion-implanted electrode, calculated for an apparent surface area, should increase in proportion to the current density $j_{non}(U)$ for a non-implanted electrode at every potential (U),

$$j_{imp}(U) = k \times j_{non}(U) \quad (1)$$

where k is a constant independent of U. This implies that the $\log j$ vs U curves for the ion-implanted and non-implanted electrodes should agree with each other by a parallel shift along the j-axis.

$$\log j_{imp}(U) = \log j_{non}(U) + \log k \quad (2)$$

However, this is not the case experimentally, as shown in Fig. 11.

The TEM and SAED investigation (Fig. 9) indicates that the ion implantation produces two surface layers, the uppermost damaged layer and the second uppermost ion-implanted layer. They also suggest that the uppermost damaged layer is composed of multi-cracked crystalline or disordered microcrystalline domains. Thus we can expect that a number of crystalline gaps of atomic sizes are produced by the ion implantation near the electrode surface. Such gaps can act as active sites for oxygen evolution, as explained in the Introduction section (see also Fig. 1), leading to the lowering of the overvoltage. Further detailed discussions on the defect structure and activation mechanism are difficult on the basis of the present experiments with the nanocrystalline film electrodes, for which a variety of defects with different structures and properties may be produced by the ion implantation. Studies with single crystal RuO_2 electrodes are necessary to get a definite conclusion on these points.

It may be interesting to note in the above respect that much larger negative shifts in the j–U curves are observed in the regions of the lower current densities in Figs. 3 and 4. This result is in harmony with the consideration that the larger negative shift is caused by the more active sites of a smaller density. If this is the case, we can expect that a much larger lowering of the overvoltage is obtained by controlling the defect structure at the surface so as to increase the density of such more active sites.

In conclusion, the present work has revealed that the ion implantation causes negative shifts of the j–U curves for oxygen

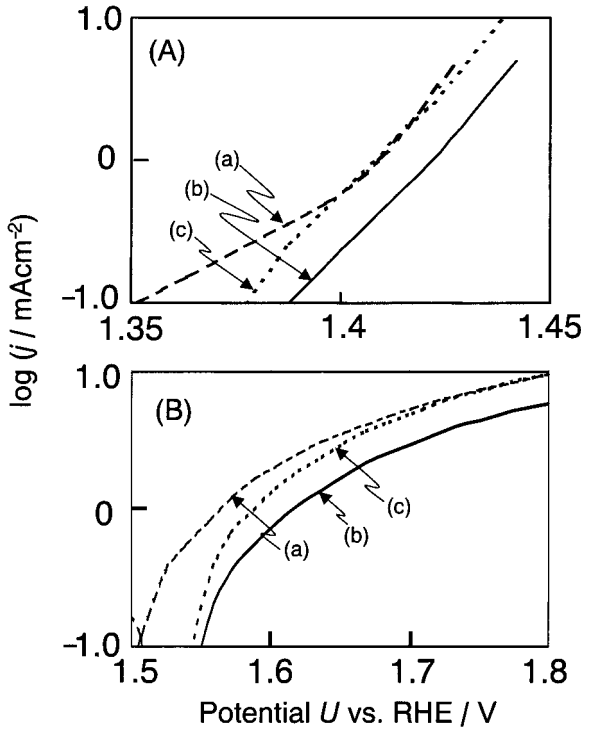

Fig. 11. (A) j–U curve (a) for a Ru^{+}-ion implanted RuO_2 film electrode (10 kV, 5.0×10^{15} cm^{-2}), compared with that (b) for non-implanted RuO_2. Curve (c) is an upward shift of curve (b) along the j-axis. (B) The same as above for Co^{+}-ion implanted (10 kV, 5.0×10^{15} cm^{-2}) and non-implanted $Ru_{2/3}Ti_{1/3}O_2$ film electrodes.

evolution on nanocrystalline metal oxide electrodes, indicating the lowering of the overvoltage for oxygen evolution. The analyses of the electrochemical behavior and the surface structure of ion-implanted electrodes have shown that the lowering of the overvoltage is neither due to a change in the chemical composition of the electrode surface nor due to an increase in the effective area of the electrode surface, but rather is due to production of certain crystal defects such as atomic gaps acting as active sites. The result is of interest, indicating that the control of defect structures near the electrode surface is a promising approach for the improvement of the oxygen evolution activity.

This work was supported partly by funding from NEDO (the New Energy and Industrial Technology Development Organization) in Japan and partly by a Grant-in-Aid for Scientific Research on Priority Area of Electrochemistry of Ordered Interfaces (No. 09237105) from the Ministry of Education, Culture, Sports, Science and Technology.

References

1 S. Trasatti, *Adv. Electrochem. Electrochem. Eng.*, **21**, 1 (1990).
2 S. Trasatti and G. Buzzanca, *J. Electroanal. Chem.*, **29**, App. 1 (1971).
3 S. Trasatti and W. E. O'Grady, *Adv. Electrochem. Electrochem. Eng.*, **12**, 177 (1981).
4 L. D. Burke, O. J. Murphy, J. F. O'Neill, and S. Venkatesan, *J. Chem. Soc., Faraday Trans. 1*, **1**, 1659 (1977).
5 S. Licht, B. Wang, S. Mukerji, T. Soga, M. Umeno, and H. Tributsch, *J. Phys. Chem. B*, **104**, 8920 (2000).
6 M. Musiani and P. Guerriero, *Electrochim. Acta*, **44**, 1499 (1998).
7 E. Rios, J.-L. Gautier, G. Poillerat, and P. Chartier, *Electrochim. Acta*, **44**, 1491 (1998).
8 J. P. Singh, N. K. Singh, and R. N. Singh, *Int. J. Hydrogen Energy*, **24**, 433 (1999).
9 T. Pauporte, F. Andolfatto, and R. Durand, *Electrochim. Acta*, **45**, 431 (1999).
10 J. Ponce, J. L. Rehspringer, G. Poillerat, and J. L. Gautier, *Electrochim. Acta*, **46**, 3373 (2001).
11 S. P. Singh, R. N. Singh, G. Poillearat, and P. Chartier, *Int. J. Hydrogen Energy*, **20**, 203 (1995).
12 G. Lodi, E. Sivieri, A. de Battisti, and S. Trasatti, *J. Appl. Electrochem.*, **8**, 135 (1978).
13 P. W. T. Lu and S. Srinivasan, *J. Electrochem. Soc.*, **125**, 1416 (1978).
14 C. Iwakura, M. Inai, and H. Tamura, *Chem. Lett.*, **1979**, 225.
15 C. Iwakura, K. Hirao, and H. Tamura, *Electrochim. Acta*, **22**, 329 (1977).
16 C. Iwakura, H. Tada, and H. Tamura, *Electrochim. Acta*, **22**, 335 (1977).
17 J. Melsheimer and D. Ziegler, *Thin Solid Films*, **163**, 301 (1988).
18 K. Izumiya, E. Akiyama, H. Habazaki, N. Kumagai, A. Kawashima, and K. Hashimoto, *Electrochim. Acta*, **43**, 3303 (1998).
19 Y. Nakato and H. Tsubomura, *Denki Kagaku* (in English), **57**, 1108 (1989).
20 Y. Nakato, H. Akanuma, Y. Magari, S. Yae, J. Shimizu, and H. Mori, *J. Phys. Chem.*, **101**, 4934 (1997).
21 Y. Magari, H. Ochi, S. Yae, and Y. Nakato, "ACS Symp. Series 656: Solid-Liquid Electrochemical Interfaces," ACS, Washington DC (1997), Chapt. 21.
22 J. P. Birsack and L. G. Haggmark, *Nucl. Instru. Methods*, **174**, 257 (1980).
23 J. F. Ziegler, J. P. Birsack, and U. Littmark, "The Stopping and Range of Ions in Solids," Pergamon, New York (1985).
24 L. A. Giannuzzi and F. A. Stevie, *Micron*, **30**, 197 (1999).
25 P. D. Townsend, J. C. Kelly, and N. E. W. Hartley, "Ion Implantation, Sputtering and their Applications," Academic Press, New York (1976).